Journal of Environmental Management 351 (2024) 119761

Contents lists available at ScienceDirect

Journal of Environmental Management

journal homepage: www.elsevier.com/locate/jenvman

Research article

Effects of CO_2 concentration and time on algal biomass film, NO3–N concentration, and pH in the membrane bioreactor: Simulation-based ANN, RSM and NSGA-II

Abdelfattah Amari [a], Noureddine Elboughdiri [b,c], Esraa Ahmed Said [d], Sasan Zahmatkesh [e,f,h], Bing-Jie Ni [g,*]

[a] Department of Chemical Engineering, College of Engineering, King Khalid University, Abha, 61411, Saudi Arabia
[b] Chemical Engineering Department, College of Engineering, University of Ha'il, P.O. Box 2440, Ha'il, 81441, Saudi Arabia
[c] Chemical Engineering Process Department, National School of Engineers Gabes, University of Gabes, Gabes, 6029, Tunisia
[d] Department of Dentistry, Al-Noor University College, Nineveh, Iraq
[e] Tecnologico de Monterrey, Escuela de Ingeniería y Ciencias, Mexico
[f] Faculty of Health and Life Sciences, INTI International University, 71800, Nilai, Negeri Sembilan, Malaysia
[g] School of Civil and Environmental Engineering, The University of New South Wales, Sydney, NSW, 2052, Australia
[h] Tecnologico de Monterrey, School of Engineering and Science, Puebla, Mexico

ARTICLE INFO

Handling Editor: Lixiao Zhang

Keywords:
Algal biomass
Membrane bioreactor
CO2 concentration
Nitrate nitrogen concentration
Artificial intelligence
Response surface method
Wastewater

ABSTRACT

The practice of aquaculture is associated with the generation of a substantial quantity of effluent. Microalgae must effectively assimilate nitrogen and phosphorus from their surrounding environment for growth. This study modeled the algal biomass film, NO_3–N concentration, and pH in the membrane bioreactor using the response surface methodology (RSM) and an artificial neural network (ANN). Furthermore, it was suggested that the optimal condition for each parameter be determined. The results of ANN modeling showed that ANN with a structure of 5-3 and employing the transfer functions tansig-logsig demonstrated the highest level of accuracy. This was evidenced by the obtained values of coefficient (R^2) = 0.998, R = 0.999, mean squared error (MAE) = 0.0856, and mean square error (MSE) = 0.143. The ANN model, characterized by a 5-5 structure and employing the tansig-logsig transfer function, demonstrates superior accuracy when predicting the concentration of NO_3–N and pH. This is evidenced by the high values of R^2 (0.996), R (0.998), MAE (0.00162), and MSE (0.0262). The RSM was afterward employed to maximize the performance of algal film biomass, pH levels, and NO_3–N concentrations. The optimal conditions for the algal biomass film were a concentration of 2.884 mg/L and a duration of 6.589 days. Similarly, the most favorable conditions for the NO_3–N concentration and pH were 2.984 mg/L and 6.787 days, respectively. Therefore, this research uses non-dominated sorting genetic algorithm II (NSGA II) to find the optimal NO3–N concentration, algal biomass film, and pH for product or process quality. The region has the greatest alkaline pH and lowest NO_3–N content.

1. Introduction

Biomass from algae can be used to manufacture nutritional supplements, renewable fuels, and wastewater treatment (Hussain et al., 2021). There has been considerable interest worldwide in microalgae in recent years, especially due to their benefits in biofuel production (Banerjee et al., 2023); for example, they are high-yielding, have high lipid concentrations, and are capable of growing rapidly. Microalgae have been found to produce fatty acids that can be used to produce biofuels, but the cost of harvesting the biomass limits its commercialization. In addition, microalgae have the capacity to perform photosynthesis, converting light energy into carbohydrates, while also engaging in the biosynthesis of proteins, lipids, and other compounds via several metabolic pathways (Su et al., 2023). Microalgae have a wide range of uses that include several fields, such as aquaculture, food production, biodiesel generation, agricultural fertilizer manufacture, and other associated disciplines (Amaro et al., 2023). On the other hand, Fig. 1 demonstrates the link between wastewater, microalgae, machine

* Corresponding author.
E-mail address: bingjieni@gmail.com (B.-J. Ni).

https://doi.org/10.1016/j.jenvman.2023.119761
Received 16 October 2023; Received in revised form 24 November 2023; Accepted 3 December 2023
Available online 19 December 2023

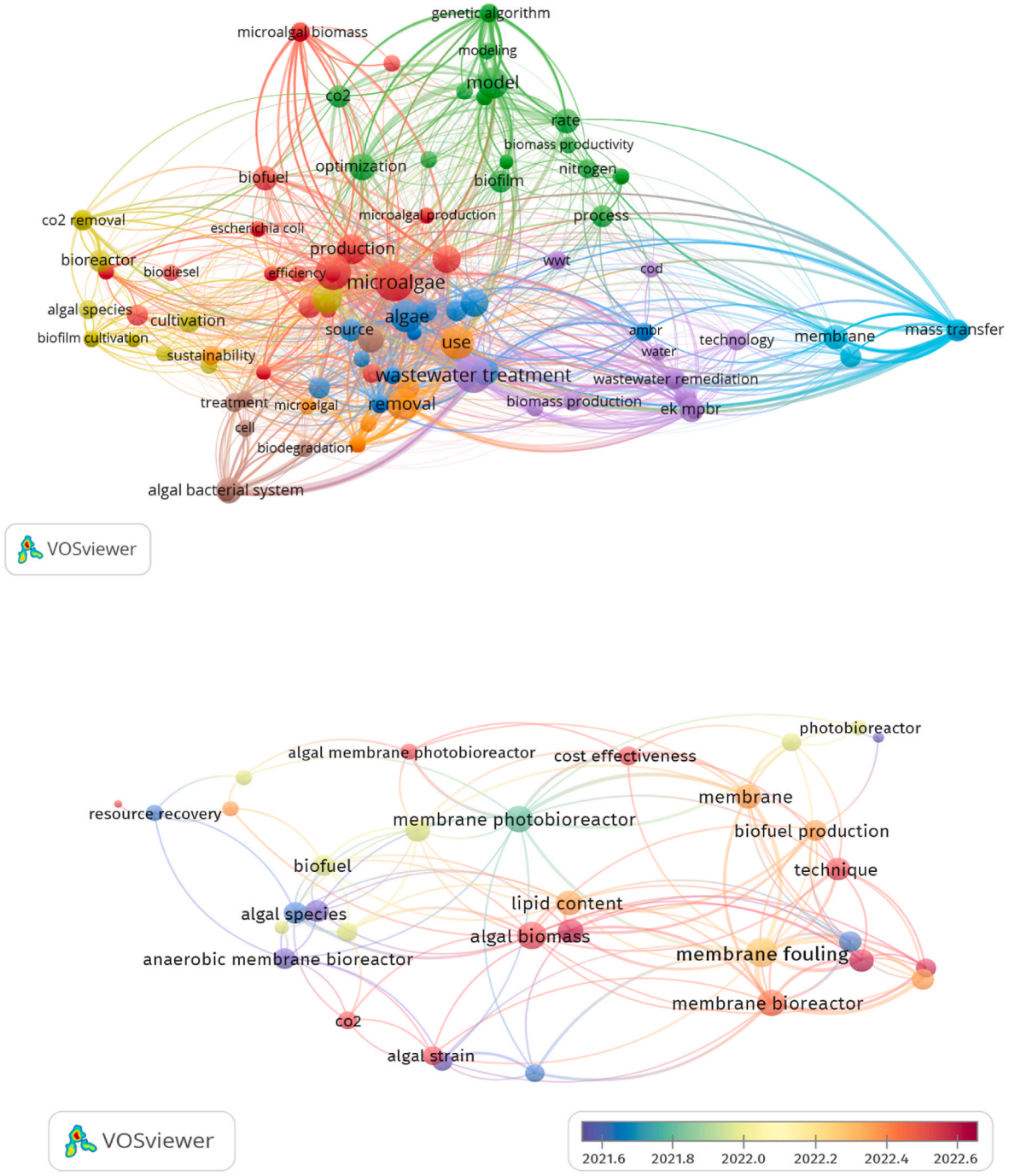

Fig. 1. Several keywords are visualized in published research using the Web of Science (e.g., wastewater, microalgae, machine learning, and bioenergy).

learning, and bioenergy. The evaluation was conducted using the VOSViewer software. By searching the Web of Science for the keywords "wastewater, microalgae, bioenergy, and machine learning," the results were found.

Algal biomass can be produced by suspension cultivation and immobilization cultivation (Garbowski et al., 2020). Among the main cultivation systems for suspension cultivation, there are open raceway ponds and closed photobioreactors (PBRs) (Yen et al., 2019). Although suspension cultivation of algal biomass is inexpensive, some disadvantages exist, such as the low productivity of the biomass, the lengthy process of cultivation, potential environmental degradation, and the cost of collecting the biomass. A closed PBR is capable of high biomass concentrations due to the higher photosynthetic efficiency of algal cells (Gupta et al., 2015). In addition, optimizing the operation conditions in the suspension culture mode can further improve bioreactor performance. Despite its advantages, suspension cultivation has a number of limitations, including high costs of biomass collection and bubble disruptions that hinder biomass growth.

Recently, there have been proposals to circumvent these limitations using biofilm-based cultivation systems, in which algal cells attach themselves to the surface of the substrate and form a biofilm. In PBRs based on biofilms, microalgae cells are immobilized specifically to reduce harvesting costs and increase biomass productivity (Mantzorou and Ververidis, 2019). Furthermore, algal biofilms offer several advantages over conventional cultivation techniques, including enhanced CO_2 mass transfer and higher environmental adaptation capacity. Moreover,

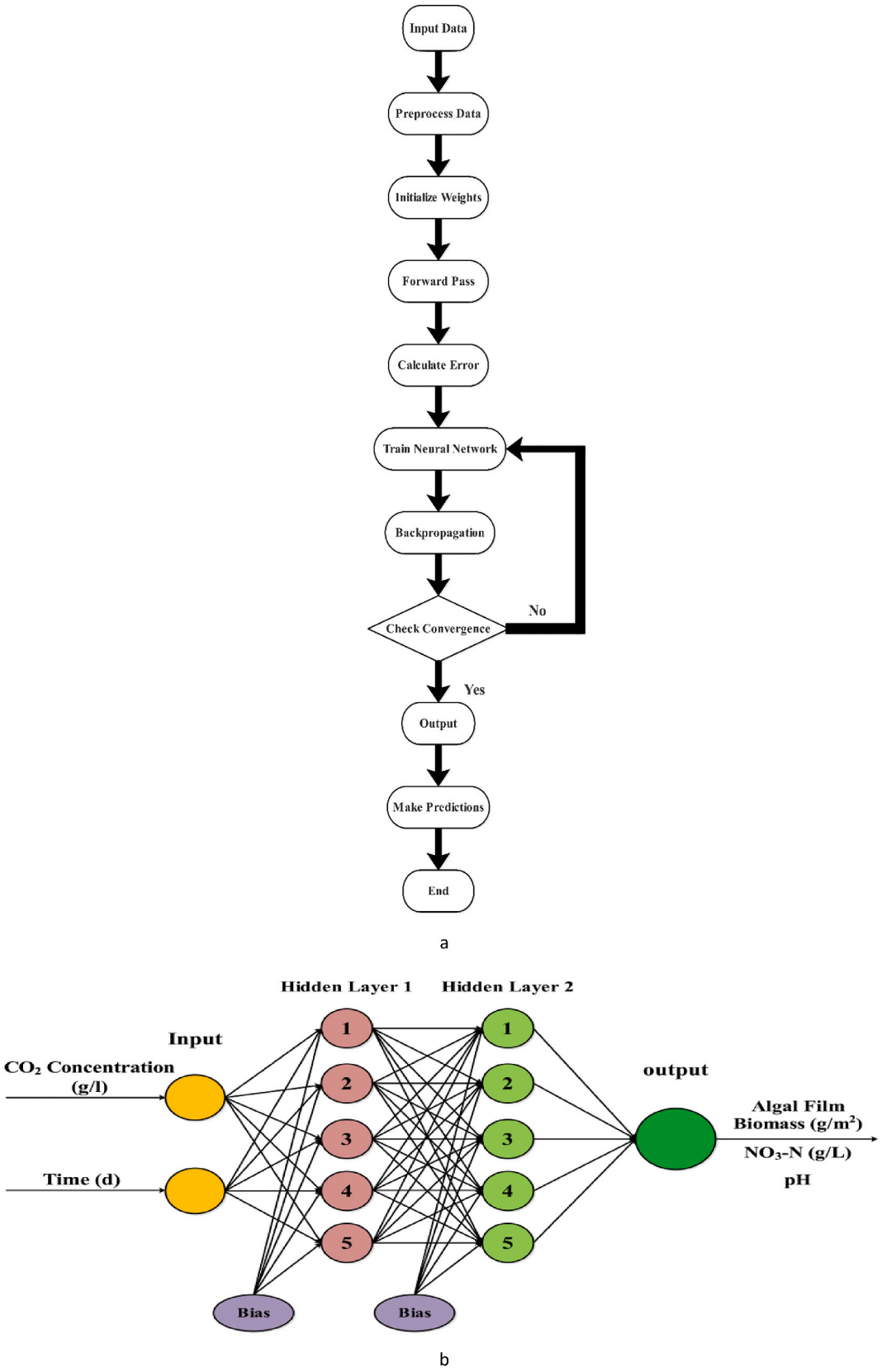

Fig. 2. a) the flowchart depicting the construction and operation of an ANN, b) Depicts the design of the artificial neural network structure.

Table 1a
ANOVA results for algal biomass film.

Source	Sum of Squares	df	Mean Square	F-value	p-value	
Model	1484.24	14	106.02	283.27	<0.0001	significant
A-Carbon dioxide concentration	8.05	1	8.05	21.50	0.0002	
B-Time	130.11	1	130.11	347.63	<0.0001	
AB	0.8637	1	0.8637	2.31	0.1444	
A^2	0.3851	1	0.3851	1.03	0.3226	
B^2	19.67	1	19.67	52.56	<0.0001	
A^2B	11.52	1	11.52	30.78	<0.0001	
AB^2	3.21	1	3.21	8.59	0.0083	
A^3	12.39	1	12.39	33.09	<0.0001	
B^3	1.62	1	1.62	4.34	0.0502	
A^2B^2	21.78	1	21.78	58.18	<0.0001	
A^3B	0.2438	1	0.2438	0.6514	0.4291	
AB^3	0.1824	1	0.1824	0.4873	0.4932	
A^4	1.44	1	1.44	3.85	0.0639	
B^4	1.50	1	1.50	4.00	0.0593	
Residual	7.49	20	0.3743			
Cor Total	1491.72	34				
Std. Dev.	0.6118		**R^2**	0.9950	**PRESS**	27.84
Mean	18.29		**Adjusted R^2**	0.9915	**−2 Log Likelihood**	45.34
C.V. %	3.35		**Predicted R^2**	0.9813	**BIC**	98.67
			Adeq Precision	55.3385	**AICc**	100.60

Table 1b
ANOVA results for NO_3–N concentration.

Source	Sum of Squares	df	Mean Square	F-value	p-value	
Model	2.88	14	0.2059	185.23	<0.0001	**significant**
A-Carbon dioxide concentration	0.0211	1	0.0211	18.94	0.0002	
B-Time	0.2822	1	0.2822	253.81	<0.0001	
AB	0.0018	1	0.0018	1.63	0.2139	
A^2	0.0095	1	0.0095	8.58	0.0071	
B^2	0.0283	1	0.0283	25.43	<0.0001	
A^2B	0.0059	1	0.0059	5.32	0.0296	
AB^2	0.0026	1	0.0026	2.34	0.1387	
A^3	0.0214	1	0.0214	19.21	0.0002	
B^3	0.0083	1	0.0083	7.45	0.0115	
A^2B^2	0.0077	1	0.0077	6.89	0.0146	
A^3B	0.0026	1	0.0026	2.30	0.1417	
AB^3	0.0002	1	0.0002	0.2138	0.6478	
A^4	0.0044	1	0.0044	3.98	0.0572	
B^4	0.0055	1	0.0055	4.99	0.0347	
Residual	0.0278	25	0.0011			
Cor Total	2.91	39				
Std. Dev.	0.0333		**R^2**	0.9905	**PRESS**	0.0974
Mean	1.01		**Adjusted R^2**	0.9851	**−2 Log Likelihood**	−177.36
C.V. %	3.30		**Predicted R^2**	0.9665	**BIC**	−122.03
			Adeq Precision	41.9263	**AICc**	−127.36

algae biofilms are known to have high photoconversion efficiency. Recent reports have described revolving biofilm reactors and twin-layer photo-bioreactors on a prototype scale (Schultze et al., 2015). Biofilm-based cultivation systems can yield low harvesting costs and increase biomass production. Disturbing the algal cell growth and adsorption of CO_2 is challenging due to the shear stress caused by CO_2 bubbles (Zhang et al., 2018). However, bio-processes based on membranes can be carried out with algae in some studies. In a wastewater treatment bioreactor using algae, the biomass is used as a soundproofing biofilm, and a light-driven photo-membrane bioreactor was also developed using algae (Asrami et al., 2023). Sonication of biomass can easily extract carbohydrates, proteins, and lipids from many algal strains (Yang et al., 2023).

Numerous research investigations have examined the utilization of artificial neural networks (ANN) (Ahmad, 2022, Gasparin et al., 2022; Khan et al., 2022), response surface methodology (RSM), machine learning (Wang et al., 2020; Zhang et al., 2022), deep learning (Hu et al., 2022, Aikhuele, 2023) and multi-objective optimization in various experimental contexts. The abovementioned algorithms have been employed to construct models, generate forecasts, and enhance the process and procedure. In this context, Hazrati et al. (2017) employed ANN to assess the efficacy of fouling management in membrane bioreactors when treating petrochemical effluent. The researchers discovered that the optimal configuration consisted of 17 neurons in the hidden layer and two neurons in the output layer. The sensitivity analysis results indicate that the mixed liquid suspended solid (MLSS) parameter has the highest transmembrane pressure (TMP) sensitivity, whereas time has the lowest sensitivity (Hazrati et al., 2017). In a separate investigation, Schmitt et al. (2017) conducted a comprehensive analysis of multiple papers on the utilization of ANN to optimize membrane bioreactors (Schmitt and Do, 2017). In a separate investigation, Chen et al. (2021) employed ANN as a predictive tool for estimating the viscosity of microalgae slurry during hydrolysis. The researchers observed a high level of agreement between the ANN model and the experimental data (Chen et al., 2021).

Furthermore, based on the evaluation metrics such as coefficient (R^2), mean square error (MSE), and MAE, it can be concluded that the ANN model exhibited high accuracy (Meng et al., 2022). The findings of

Table 1c
ANOVA results for pH.

Source	Sum of Squares	df	Mean Square	F-value	p-value	
Model	26.51	14	1.89	97.22	<0.0001	**significant**
A-Carbon dioxide concentration	1.86	1	1.86	95.32	<0.0001	
B-Time	0.8761	1	0.8761	44.98	<0.0001	
AB	0.2669	1	0.2669	13.71	0.0011	
A^2	0.6057	1	0.6057	31.10	<0.0001	
B^2	0.2962	1	0.2962	15.21	0.0006	
A^2B	0.0262	1	0.0262	1.35	0.2569	
AB^2	0.0409	1	0.0409	2.10	0.1595	
A^3	1.49	1	1.49	76.34	<0.0001	
B^3	0.0085	1	0.0085	0.4369	0.5147	
A^2B^2	0.0141	1	0.0141	0.7251	0.4026	
A^3B	0.1362	1	0.1362	7.00	0.0139	
AB^3	0.0003	1	0.0003	0.0133	0.9092	
A^4	0.6088	1	0.6088	31.26	<0.0001	
B^4	0.0748	1	0.0748	3.84	0.0613	
Residual	0.4869	25	0.0195			
Cor Total	26.99	39				
Std. Dev.	0.1396		**R^2**	0.9820	**PRESS**	1.67
Mean	8.09		**Adjusted R^2**	0.9719	**−2 Log Likelihood**	−62.83
C.V. %	1.73		**Predicted R^2**	0.9382	**BIC**	−7.50
			Adeq Precision	31.2723	**AICc**	−12.83

their study demonstrated the feasibility of utilizing ANN models to evaluate the viscosity of microalgae slurry. Pendashteh et al. (2011) employed ANN to simulate membrane bioreactors in a separate investigation. The researchers discovered that at an organic loading rate (OLR) of 2.44 kg chemical oxygen demand (COD) per day per cubic meter, the total dissolved solids (TDS) concentration reached 78,000 mg/L, and the reaction duration was 40 h, resulting in an average COD elimination efficiency of 98%. Under these circumstances, the concentration of COD in the effluent was found to be below 100 mg/L, which is below the permissible limits for discharge (Pendashteh et al., 2011).

Furthermore, Schmitt et al. (2018) employed ANN as a predictive tool for membrane fouling in membrane bioreactors (MBRs). A total of ten distinct parameters were included as inputs to the ANN architecture. The researchers concluded that ANNs have significant potential for effectively addressing this application (Schmitt et al., 2018). Ibrahim et al. (2020) employed ANN to optimize membrane bioreactors. The researchers discovered that the ANN demonstrates a high level of accuracy in predicting the permeate flux of membrane bioreactor filtration (Ibrahim et al., 2020).

The primary objective of the current investigation is to develop a model that can accurately predict and optimize the behavior of algal film biomass, pH, and NO_3–N concentration in a membrane bioreactor. The acquisition of process data has been accomplished by research conducted by Zhang et al. (2018) (Zhang et al., 2018). The experimental condition involved exposing the samples to a range of CO_2 concentrations, specifically varying from 0% to 10%, for a duration from 0 to 7 days. Initially, the behavior of algal film biomass, pH, and NO_3–N concentration was modeled using the RSM. Subsequently, the parameters mentioned above are represented using ANN. An ANN's optimal architecture has been selected to model the behavior of algal film biomass, pH, and NO_3–N concentration. The optimization of algal film biomass, pH, and NO_3–N concentration behavior has been successfully achieved by implementing RSM.

2. Material and methods

2.1. Response surface methodology (RSM)

The RSM is a robust statistical technique widely employed in various scientific and engineering domains to optimize and model intricate systems effectively. The creation of RSM in the mid-twentieth century has rendered it an indispensable instrument for researchers and engineers in the execution of experiments, exploration of connections among several components, and achievement of optimal outcomes with limited resources. The fundamental concept underlies RSM is constructing an approximation of a system's response surface. This approximation enables researchers to predict the ideal settings for factors, determine the significant impact variables, and explore the system's behavior within the experimental region (Bezerra et al., 2008).

One of the critical features of RSM is its ability to effectively manage intricate and non-linear relationships among variables. The RSM utilizes a polynomial model to estimate the proper response surface inside the experimental region by conducting a series of experimental runs. This enables researchers to enhance the system's performance without incurring the expenses and time constraints of conducting elaborate tests. Moreover, the RSM enables the integration of linear and quadratic effects, rendering it well-suited for assessing intricate systems characterized by higher-order interactions. Due to its versatile nature, the utilization of RSM is prevalent across diverse sectors, including chemical engineering, manufacturing, agriculture, and medicine (Myers et al., 2004).

Despite the numerous advantages of RSM, certain limitations need to be acknowledged. The model's accuracy heavily depends on selecting an experimental design and assuming a response surface that behaves predictably. Undesirable consequences may arise as a consequence of deviations from these principles. Consequently, researchers must exercise caution in interpreting the model's predictions and diligently verify the outcomes by supplementary testing. However, when implemented and assessed correctly, the RSM is essential for optimizing intricate systems, generating valuable insights, and advancing scientific and engineering research (Kleijnen, 2008).

2.2. Artificial neural networks (ANN)

The utilization of ANNs, derived from investigating the human brain, has emerged as a computational instrument in various scientific and technical fields. This study employs an ANN approach to model and forecast the relationship among multiple variables inside an experimental setting. ANN architectures consist of interconnected networks organized hierarchically. Each node inside these networks represents a neuron responsible for processing information. These neurons communicate with one another through dense connections. ANN models have the ability to effectively capture intricate correlations in data that may be challenging to visualize using traditional statistical models. This is mainly attributed to their inherent capacity to learn from and adapt to nonlinear and complex patterns within the data. In order to use the ANN

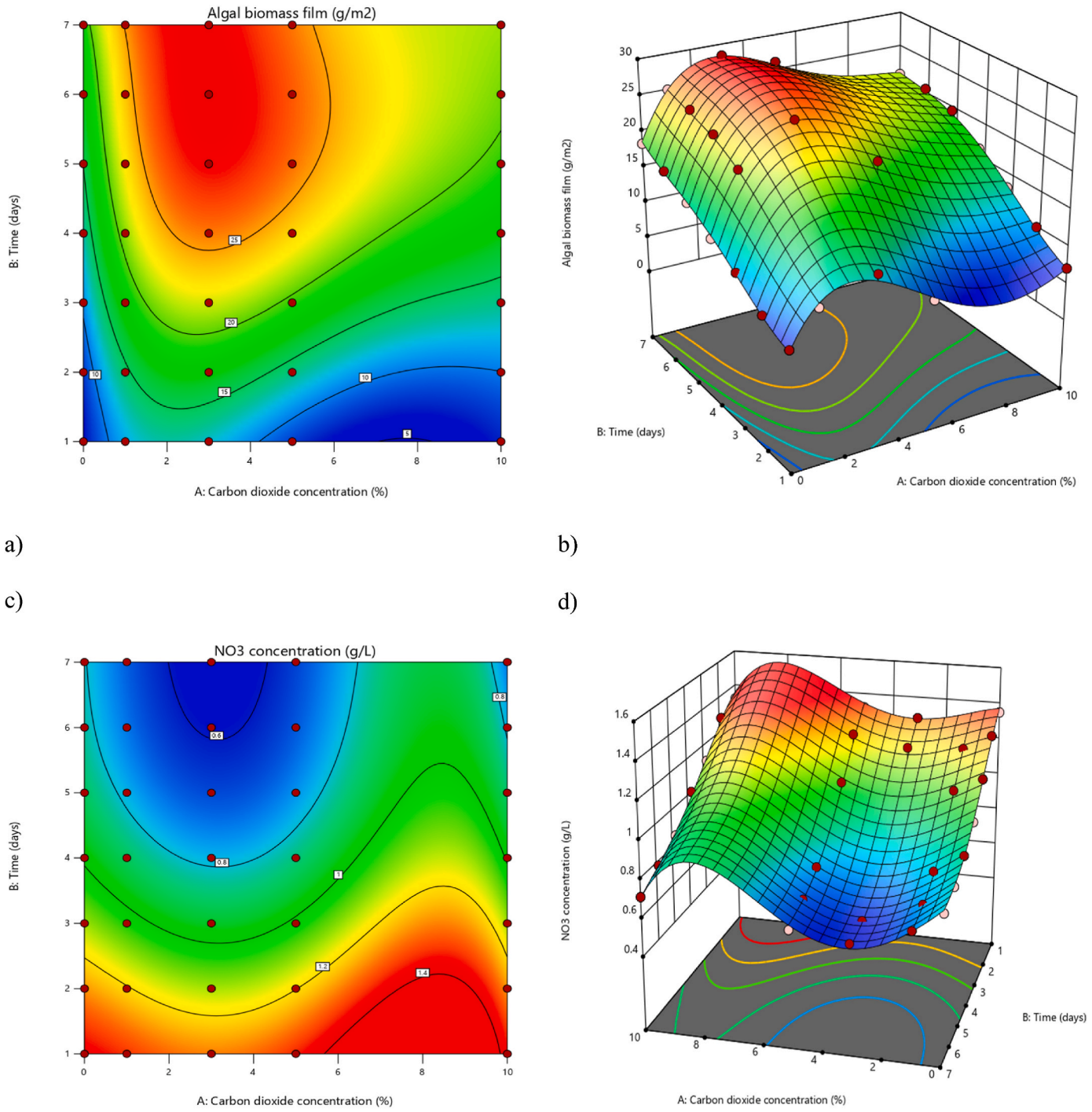

Fig. 3. Algal biomass behavior RSM model a) contour, and b) 3D graphs. NO_3–N concentration, and pH behavior RSM model c, e) contour, and d, f) 3D graphs.

methodology, it is necessary to initially collect comprehensive data, including the characteristics of the input variables and the corresponding experimental outcomes (Agatonovic-Kustrin and Beresford, 2000).

In order to enhance the performance of the model, the dataset is partitioned into many subsets that are used for training, validation, and testing objectives. Following this, the construction of the ANN model framework is undertaken. During this step, the ideal number of hidden layers and neurons is determined for each layer. The requisite function is then formulated. The backpropagation strategy is utilized in training the model, wherein the links are assigned incorrect weights, and the data is effectively utilized to minimize the error in output prediction during the training phase.

Different metrics, such as MSE and correlation R^2, were employed to assess the performance of the Trained ANN model by comparing its projected values to experimental results on test data. Furthermore, a sensitivity analysis was performed to ascertain the statistical relevance of the material in deciding the outcome (Bourquin et al., 1998).

The ANN methodology is implemented using Python and widely adopted libraries such as TensorFlow or PyTorch. Modern processing devices, specifically Graphics Processing Units (GPUs), are also leveraged to expedite training. This study aims to improve methodology by incorporating the neural network approach, a widely used technology

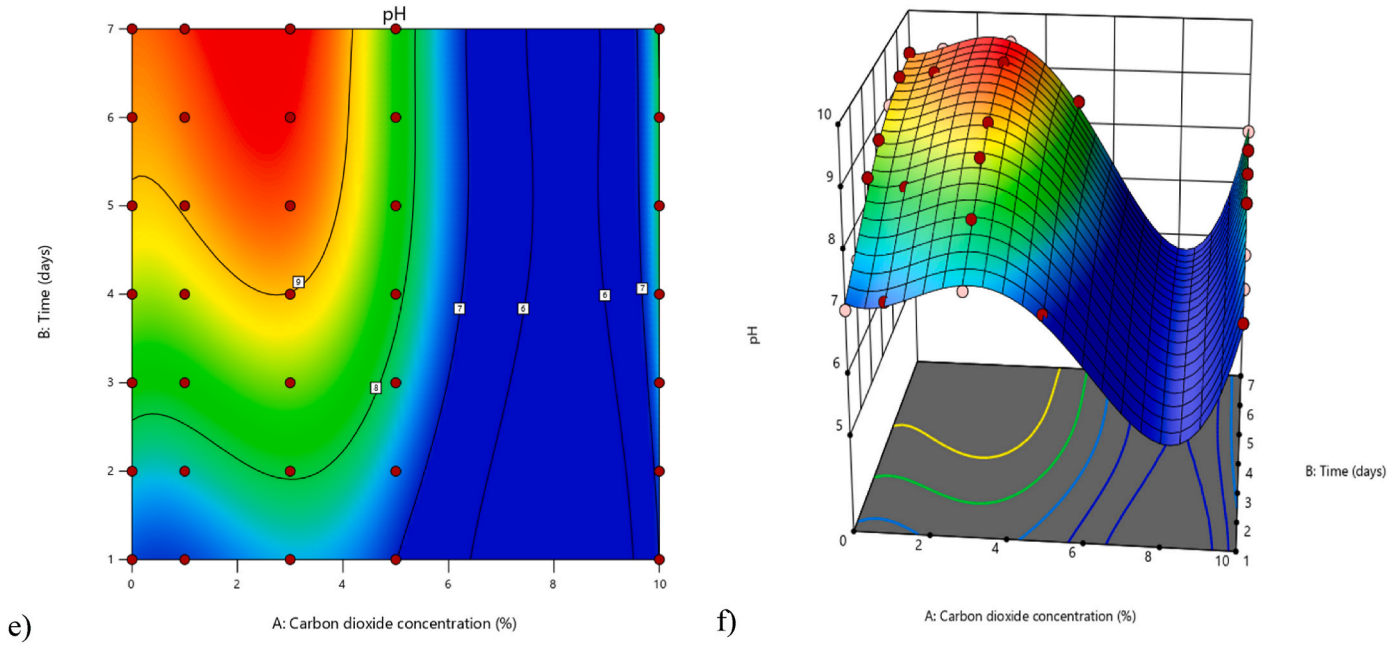

Fig. 3. (*continued*).

renowned for its rigorous investigation and real-world implementations across several domains. This methodology aims to foster a comprehensive understanding of the experimental relationships and provide precise predictions.

The flowchart of the ANN is shown in Fig. 2a. The flowchart offers a graphical representation of the respective methodologies and illustrates the sequential steps involved in the ANN process. The dataset should be gathered and organized to include input characteristics (x_1, x_2, …, xn) and their corresponding goal output (y). In order to enhance the efficiency of training, it is necessary to normalize or standardize the input data to guarantee consistency and uniformity. The connections between the input nodes and the hidden layer are assigned initial random weights (w_1, w_2, …, wn). The weighted total of inputs at each neuron in the hidden layer is computed by applying the activation function. To assess the accuracy of the model's predictions, it is necessary to compare the anticipated output with the actual target output and calculate the resulting error. The weights should be adjusted by the use of gradient descent in order to reduce the mistake. This process includes the calculation of gradients and the subsequent adjustment of weights. Determine if the model has achieved convergence conditions, such as meeting a minimum error level. Once convergence is attained, the trained model becomes prepared for making predictions. Utilize the training to generate predictions on novel, unobserved data.

As shown in Fig. 2b, this study utilizes an ANN consisting of two layers of five neurons with tansigmoid and logsimoid transfer functions. The network takes CO_2 Concentration (g/l) and Time (d) parameters as input and aims to predict the Algal Film Biomass (g/m^2), pH, and NO_3–N (g/L) target variables.

2.3. NSGA-II

The non-dominated sorting genetic algorithm II (NSGA-II) is a widely recognized approach for multi-objective optimization problems, which has been employed in this study to resolve such concerns. The NSGA-II method is a genetic algorithm extension designed to maximize several objectives and provide non-dominant solutions, previously referred to as Pareto fronts. The method operates on a population of potential solutions, each representing a set of diverse measurements for the optimization problem (Amiri et al., 2023).

The NSGA-II algorithm is utilized in this research to optimize the experimental settings when there are several conflicting objectives. Initially, the optimization problem's objectives and constraints are delineated to establish a clear and concise mathematical representation.

Afterward, random or semi-random sampling methods fill the parameter space with potential solutions, increasing the diversity. Following this, a mathematical function is used to evaluate the replies given by each candidate, and their suitability is determined by evaluating the strengths and weaknesses of their answers concerning other options. The NSGA-II selection process, when in optimal condition, upholds the principles of non-segregation and remote crowding, hence promoting diversity and a well-balanced exploration and exploitation of the search space. The candidate solutions undergo iterative adjustments to their fitness and gradually converge towards the Pareto front throughout multiple generations, facilitated by genetic interventions such as crossover and mutation. The optimization technique is iteratively employed multiple times to provide a high-quality set of non-dominant solutions that effectively capture the tradeoff inherent in the conflicting objectives of the brand (Zahmatkesh et al., 2023).

The NSGA-II algorithm is implemented in a programming language appropriate for the task, such as Python or C++. Its effectiveness is evaluated using hyper-volume, throughput, and distance metrics. This research aims to improve the understanding of multi-objective optimization in experimental and decision-making systems in various real-world contexts using the NSGA-II approach.

3. Results and discussions

3.1. RSM modeling results

This study utilizes the findings of Zhang et al. (2018) to construct a model and propose correlations for each component (Zhang et al., 2018). When expressed in terms of the actual factors, the equation enables the generation of predictions for the reaction at specific levels of each factor. It is imperative to provide explicit specifications for each factor's original units. The empirical equations presented in this study demonstrate the interdependence between algal biomass film, NO_3–N concentration, and pH. The equations established from the RSM model are founded upon time and CO_2 concentration variables. These equations forecast the behavior of algal biomass film, NO_3–N concentration, and pH. The equations were developed utilizing the quartic model.

$$Algal\ biomass\ film = +7.35886 + 5.71286\times CO_2 - 3.03818\times Time + 2.00535\times CO_2\times Time - 2.42677\times CO_2^{\,2} + 2.44420\times Time^2 - 0.166918 \times CO_2^{\,2} * Time - 0.199905\times CO_2\times Time^2 + 0.276526\times CO_2^{\,3} - 0.434100\times Time^3 + 0.021917\times CO_2^{\,2}\times Time^2 - 0.002527\times CO_2^{\,3}\times Time - 0.003667\times CO_2 \times Time^3 - 0.009117\times CO_2^{\,4} + 0.025718\times Time^4 \quad (1)$$

$$CO_2\ concentration = +1.37968 + 0.013942\times CO_2 + 0.072629\times Time - 0.039295 CO_2\times Time - 0.024502\times CO_2^{\,2} - 0.092394\times Time^2 + 0.006100 \times CO_2^{\,2}\times Time + 0.003228\times CO_2\times Time^2 + 0.007017\times CO_2^{\,3} + 0.015527\times Time^3 - 0.000291\times CO_2^{\,2}\times Time^2 - 0.000211\times CO_2^{\,3}\times Time - 0.000080\times CO_2 \times Time^3 - 0.000473\times CO_2^{\,4} - 0.000783\times Time^4 \quad (2)$$

$$pH = +6.89963 - 0.361661\times CO_2 + 0.096105\times Time + 0.062682 CO_2\times Time + 0.380231\times CO_2^{\,2} + 0.235813\times Time^2 - 0.025029 CO_2^{\,2}\times Time - 0.002423\times CO_2 \times Time^2 - 0.089716\times CO_2^{\,3} - 0.049037\times Time^3 + 0.000395\times CO_2^{\,2}\times Time^2 + 0.001543\times CO_2^{\,3}\times Time + 0.000083\times CO_2 \times Time^3 + 0.005546\times CO_2^{\,4} + 0.002874\times Time^4 \quad (3)$$

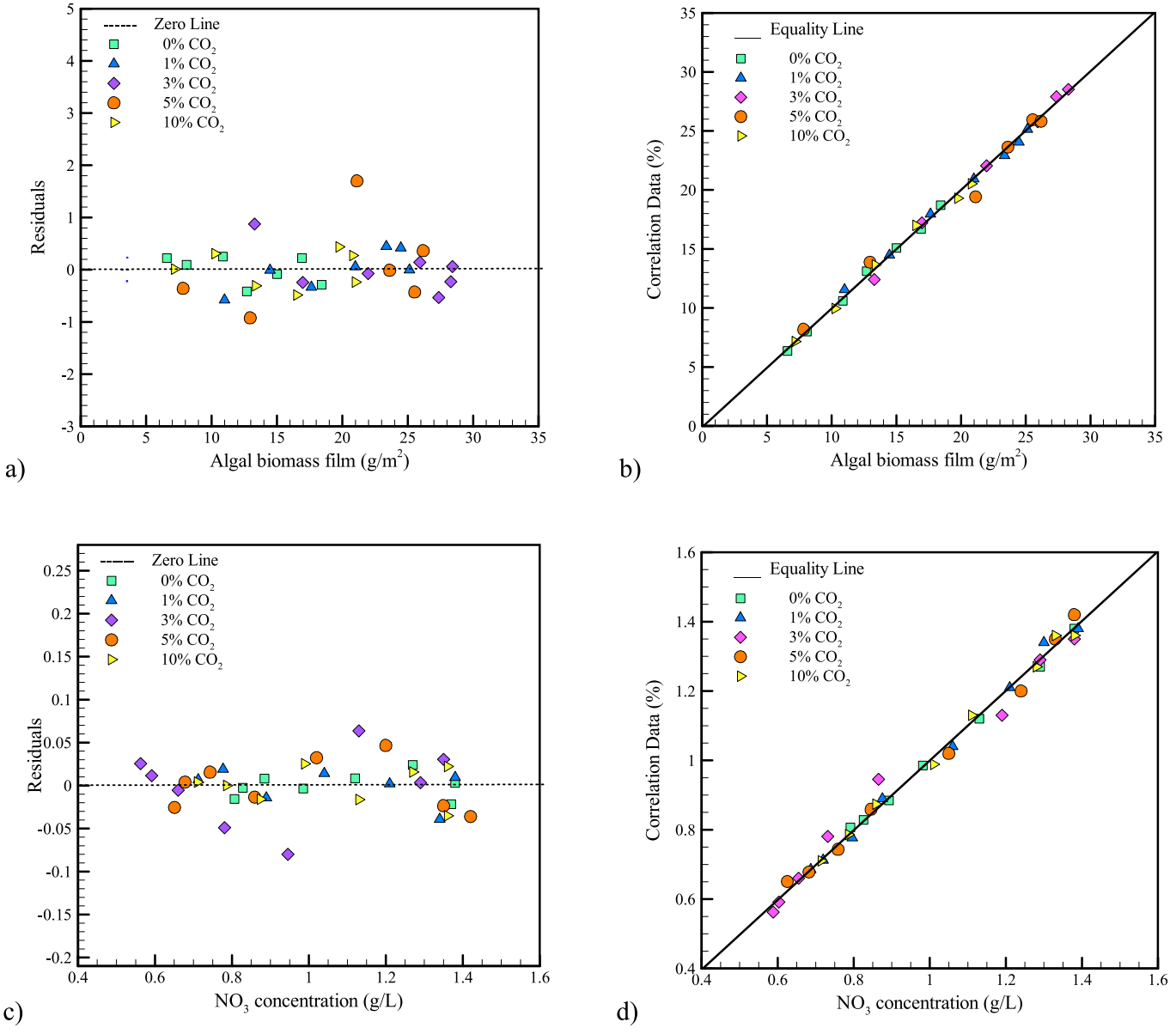

Fig. 4. Residual, and predict-actual graphs for a, b) algal biomass film, c, d) NO_3–N concentration, e, f) pH behavior.

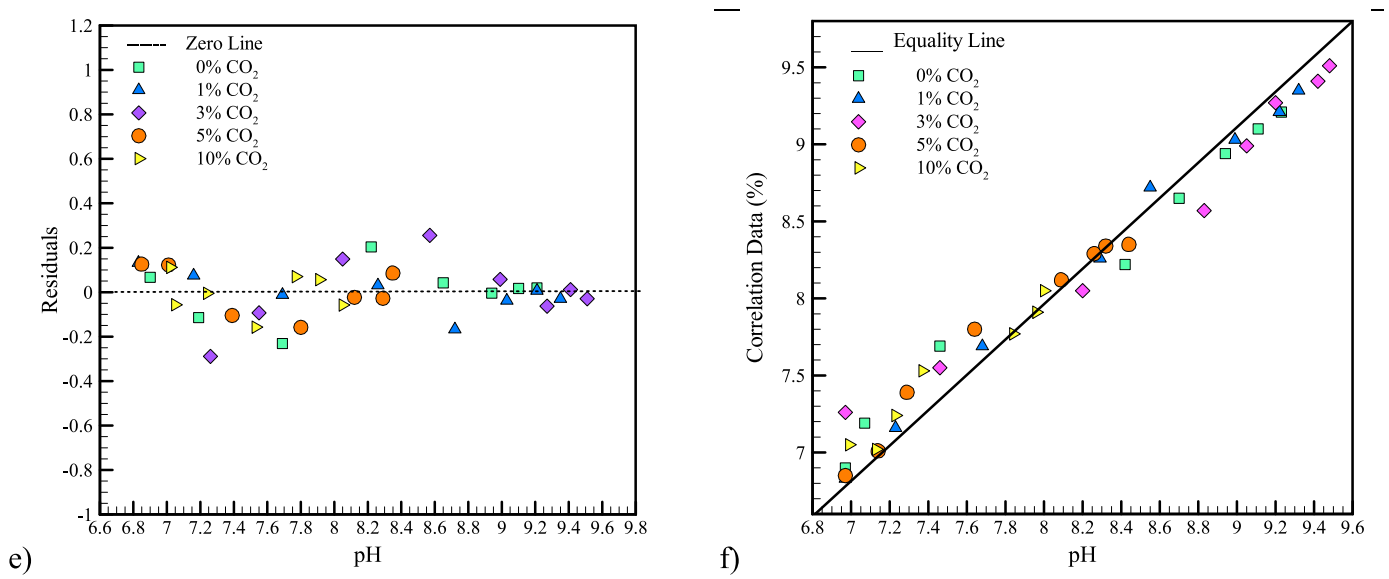

Fig. 4. (*continued*).

The analysis of variance (ANOVA) outcomes for the RSM model about the behavior of algal biomass film, NO3–N concentration, and pH are presented in Tables 1–3. Additionally, factor coding is systematically organized and standardized. Additionally, it should be noted that the sum of squares is classified as type III, specifically in the context of partial effects.

Table 1a displays the ANOVA results of the RSM model investigating the behavior of algal biomass film. The obtained F-value of 283.27 suggests that the model is statistically significant. A large F-value of this magnitude may occur due to random variation in only 0.01% of instances. The significance of model terms is established when the P-value is below the threshold of 0.0500. The essential model variables in this scenario include A, B, B^2, A^2B, AB^2, A^3, and A^2B^2. Values greater than 0.1000 indicate that the model terms lack significance. The application of model reduction techniques can be beneficial for improving a model when it has many insignificant model terms, except those essential for maintaining hierarchy. The Predicted R^2 value of 0.9813 closely approximates the Adjusted R^2 value of 0.9915, with a difference of less than 0.2. Adeq Precision conducts the measurement of the signal-to-noise ratio. A ratio over four is favored. The ratio of 55.338 indicates that the signal is sufficient. This paradigm demonstrates utility in effectively navigating the design space.

Table 1b presents the ANOVA outcomes for the RSM model according to the behavior of NO_3–N concentration. The obtained Model F-value of 185.23 suggests that the model has statistical significance. The probability of observing an F-value of this magnitude due to random variation is extremely low, at less than 0.01%. P-values below the threshold of 0.0500 indicate statistical significance for the model terms. The essential model variables in this circumstance are denoted as A, B, A^2, B^2, A^2B, A^3, B^3, A^2B^2, and B^4. Values greater than 0.1000 indicate that the model terms lack statistical significance. The application of model reduction techniques could improve the performance of a model that contains many model terms that are deemed unnecessary, except those that are essential for maintaining a hierarchical structure. The difference between the Predicted R^2 value of 0.9665 and the Adjusted R^2 value of 0.9851 is smaller than 0.2. Adeq Precision is responsible for the computation of the signal-to-noise ratio. A ratio beyond four is deemed more favorable. The ratio of 41.926 exhibits a satisfactory level of signal strength. The utilization of this paradigm has the potential to facilitate exploration inside the design space.

Table 1c presents the ANOVA outcomes for the RSM model according to the behavior of pH. The model exhibits a high significance level, evidenced by the Model F-value of 97.22. A large F-value of this magnitude may occur due to random variation in only 0.01% of instances. Model terms are deemed statistically significant if their P-values are below 0.0500. In this case, the significant model terms encompass A, B, AB, A^2, B^2, A3, A^3B, and A^4. Model terms are considered statistically insignificant if their p-value exceeds the threshold of 0.1000. The model reduction process could improve a model's performance by eliminating extraneous terms, except those necessary for maintaining hierarchical structure. The difference between the Predicted R^2 value of 0.9382 and the Adjusted R^2 value of 0.9719 is below the threshold of 0.2, indicating a reasonable level of concordance. The measurement of the signal-to-noise ratio is conducted using Adeq Precision. A minimum ratio of 4 is desired. The strength of the signal is deemed sufficient, as evidenced by the ratio of 31.272. In order to navigate through the design area, it is recommended to employ the utilization of this particular model.

A contour and three-dimensional representation of the algal biomass film can be seen in Fig. 3a and b. It has become abundantly clear that higher amounts of algal biomass film have been discovered for longer durations and in response to a wide range of CO_2 concentrations. For clarity, it has been noticed that the highest levels of algal biomass film may be achieved within four to seven days, concurrently with a concentration of carbon dioxide ranging from 1.5 to 4.5 percent. As can be seen, higher values of algal biomass film have been observed at higher times in different CO_2 concentrations. In addition, the sensitivity of algal biomass film to CO_2 is higher than time.

Fig. 3c–f displays a contour and three-dimensional graph illustrating the concentration of NO_3–N and pH. Elevated levels of NO_3–N concentration have been recorded throughout shorter periods and in the presence of greater CO_2 concentrations. To clarify, the highest levels of NO_3–N concentration were seen within 0–3 days, and when CO_2 concentration reached 6–10%. Elevated pH levels with reduced quantities of carbon dioxide have been documented for extended periods. To clarify, the uppermost pH levels have been attained within 5–7 days, accompanied by CO_2 concentrations ranging from 0 to 4%. Moreover, when exposed to elevated levels of carbon dioxide exceeding 4.5, the alterations in pH resulting from temporal variations are minimal. In addition, it observed sharp trends in pH behavior for the process.

Fig. 4a–f displays the graphical representations of the residual and actual-predict models for the behavior of algal biomass film, NO_3–N concentration, and pH. The distance between the points on the diagonal line determines the criterion for agreement between experimental and anticipated values. The degree of agreement between experimental and

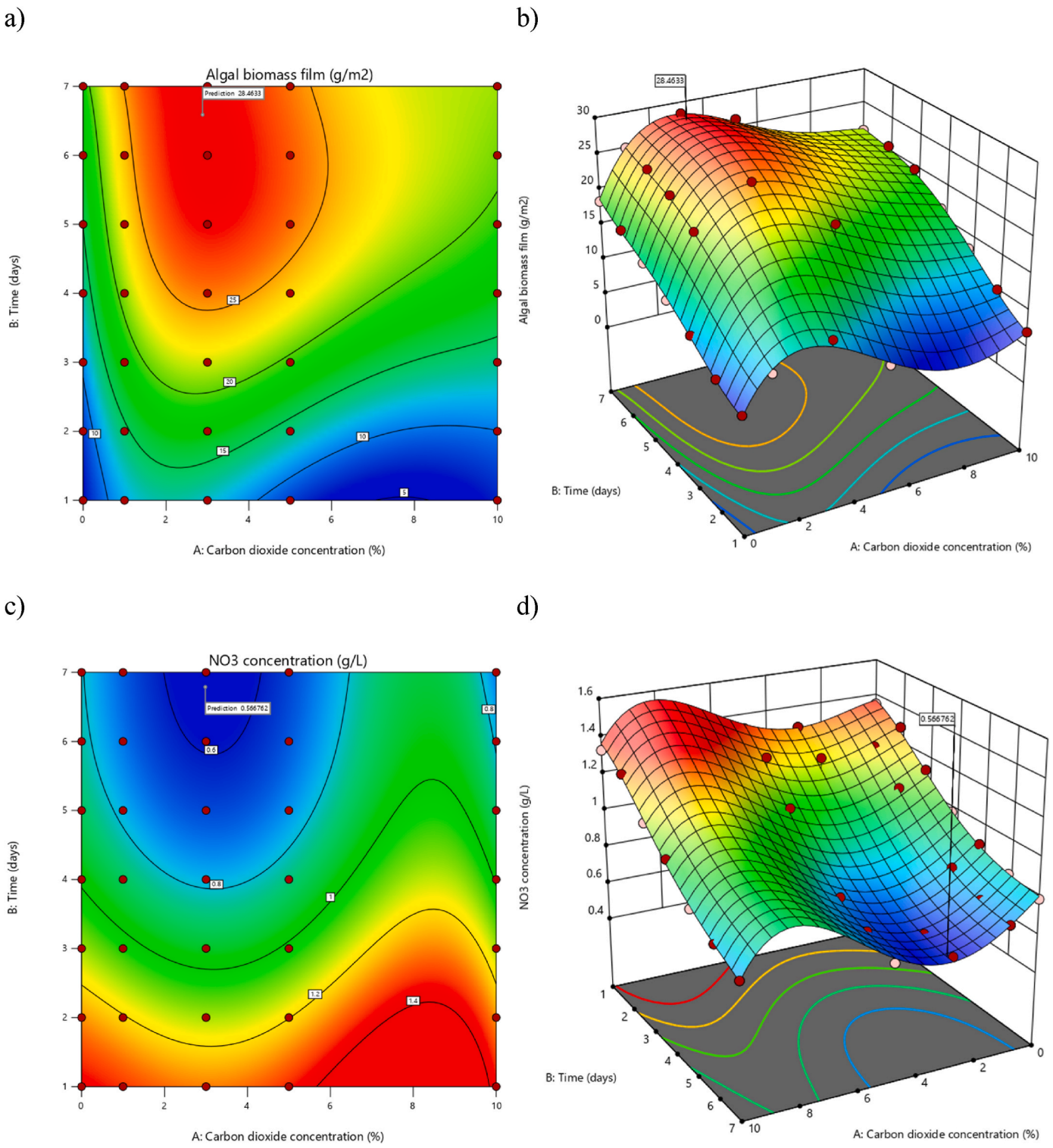

Fig. 5. Contour and 3D graphs of RSM optimization for algal biomass, NO_3–N concentration, and pH.

predicted values is determined by calculating the spacing of the dots on the diagonal line. Based on the abovementioned observations, the proposed model is notable in accurately forecasting the pH, NO_3–N concentration, and algal biomass film—the behavior of microalgae in a membrane bioreactor.

3.2. RSM optimization

The RSM method was employed to optimize the behavior of algal biomass film, NO_3–N concentration, and pH concerning time and CO_2 concentration. In this context, it is imperative to decrease the concentration of CO_2 and maximize the pH level.

Table S1 presents the ten optimal modes that were identified for the production of algal biomass films. Additionally, Table S2 presents the

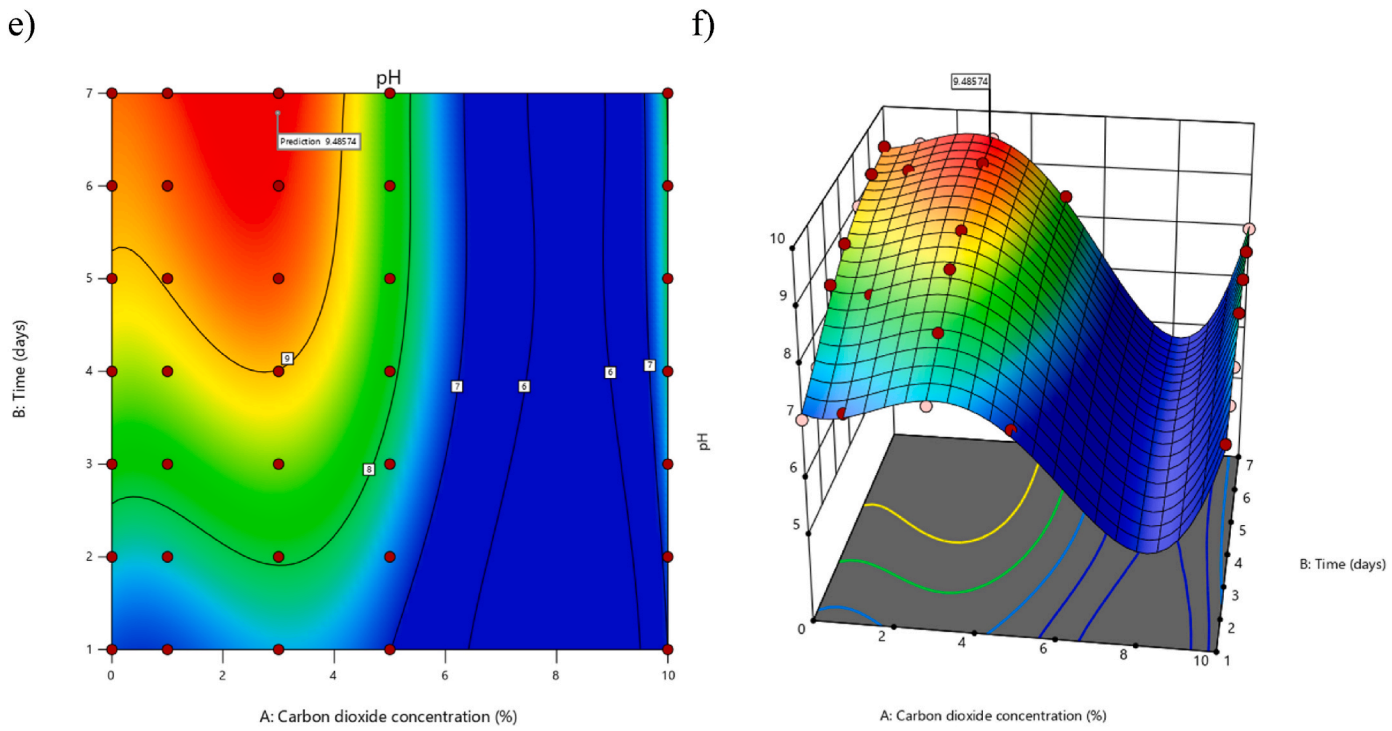

Fig. 5. (*continued*).

Table 2
Structure and accuracy parameters of artificial neural network for algal biomass film.

row	structure		transfer function		R^2	R	MAE	MSE
1	2	2	Tansig	tansig	9.94E-01	9.97E-01	2.47E-01	3.85E-01
2	2	5	Tansig	tansig	9.94E-01	9.97E-01	2.37E-01	3.36E-01
3	3	3	logsig	logsig	9.96E-01	9.98E-01	1.50E-01	1.88E-01
4	5	3	Tansig	tansig	9.97E-01	9.98E-01	1.48E-01	2.13E-01
5	**5**	**3**	**tansig**	**logsig**	**9.98E-01**	**9.99E-01**	**8.56E-02**	**1.43E-01**

ten optimal modes identified for the concentration of NO_3–N and pH. The optimal conditions for the growth of algal biomass film were seen at a carbon dioxide concentration of 2.884 mg/L and a duration of 6.589 days. Furthermore, it was observed that the most favorable conditions for achieving optimal NO_3–N concentration and pH levels were attained when the CO_2 concentration reached a value of 2.984 mg/L, and the experiment lasted 6.787 days. Fig. 5a-**f** displays contour and three-dimensional graphs depicting the RSM optimization model for the algal biomass film, NO_3–N concentration, and pH.

3.3. ANN modeling results

This part presents the introduction of ANN modeling for the experimental data of Zhang et al. (2018), explicitly focusing on algal biomass film concentration, nitrogen concentration, and pH. The inputs in this study encompassed time and carbon dioxide concentration, while the outputs consisted of algal biomass film concentration, nitrogen concentration, and pH. Table 2 displays the introduction and accuracy parameters of the ANN developed to forecast the algal biomass film. Based on the data presented in Tables 2 and it can be observed that the ANN model, characterized by a 5-3 structure and employing the tansig-logsig transfer function, exhibits the highest level of accuracy. This is evidenced by the values of R^2 (9.98E-01), R (9.99E-01), MAE (8.56E-02), and MSE (1.43E-01). Consequently, this model can predict the growth of algal biomass film effectively.

Table 3
Structure and accuracy parameters of artificial neural network NO_3–N concentration and pH.

row	structure		transfer function		R^2	R	MAE	MSE
1	1	1	tansig	tansig	7.27E-01	8.55E-01	6.79E-02	1.96E-01
2	1	1	logsig	tansig	8.23E-01	9.11E-01	6.19E-02	1.74E-01
3	1	1	logsig	logsig	8.40E-01	9.22E-01	6.15E-02	1.71E-01
4	1	3	logsig	logsig	8.45E-01	9.20E-01	5.30E-02	1.50E-01
5	1	1	tansig	tansig	8.10E-01	9.03E-01	5.29E-02	1.55E-01
6	2	1	logsig	tansig	8.18E-01	9.09E-01	4.12E-02	1.49E-01
7	2	1	tansig	logsig	7.93E-01	8.91E-01	1.26E-02	8.75E-02
8	2	2	tansig	tansig	9.36E-01	9.68E-01	9.65E-03	7.59E-02
9	2	2	logsig	logsig	9.62E-01	9.81E-01	5.99E-03	5.64E-02
10	2	3	logsig	tansig	9.74E-01	9.87E-01	3.40E-03	4.29E-02
11	2	5	logsig	tansig	9.82E-01	9.91E-01	2.41E-03	2.87E-02
12	5	3	logsig	logsig	9.74E-01	9.87E-01	1.82E-03	3.10E-02
13	**5**	**5**	**logsig**	**logsig**	**9.96E-01**	**9.98E-01**	**1.62E-03**	**2.26E-02**

Table 3 presents the parameters of the establishment and precision of the ANN developed for determining NO_3–N concentration and pH. Based on the provided Tables 3 and it can be observed that the ANN model, characterized by a 5-5 structure and employing the tansig-logsig transfer function, exhibits the highest level of accuracy. This is evidenced by the values of R^2 (9.96E-01), R (9.98E-01), MAE (1.62E-03), and MSE (2.62E-

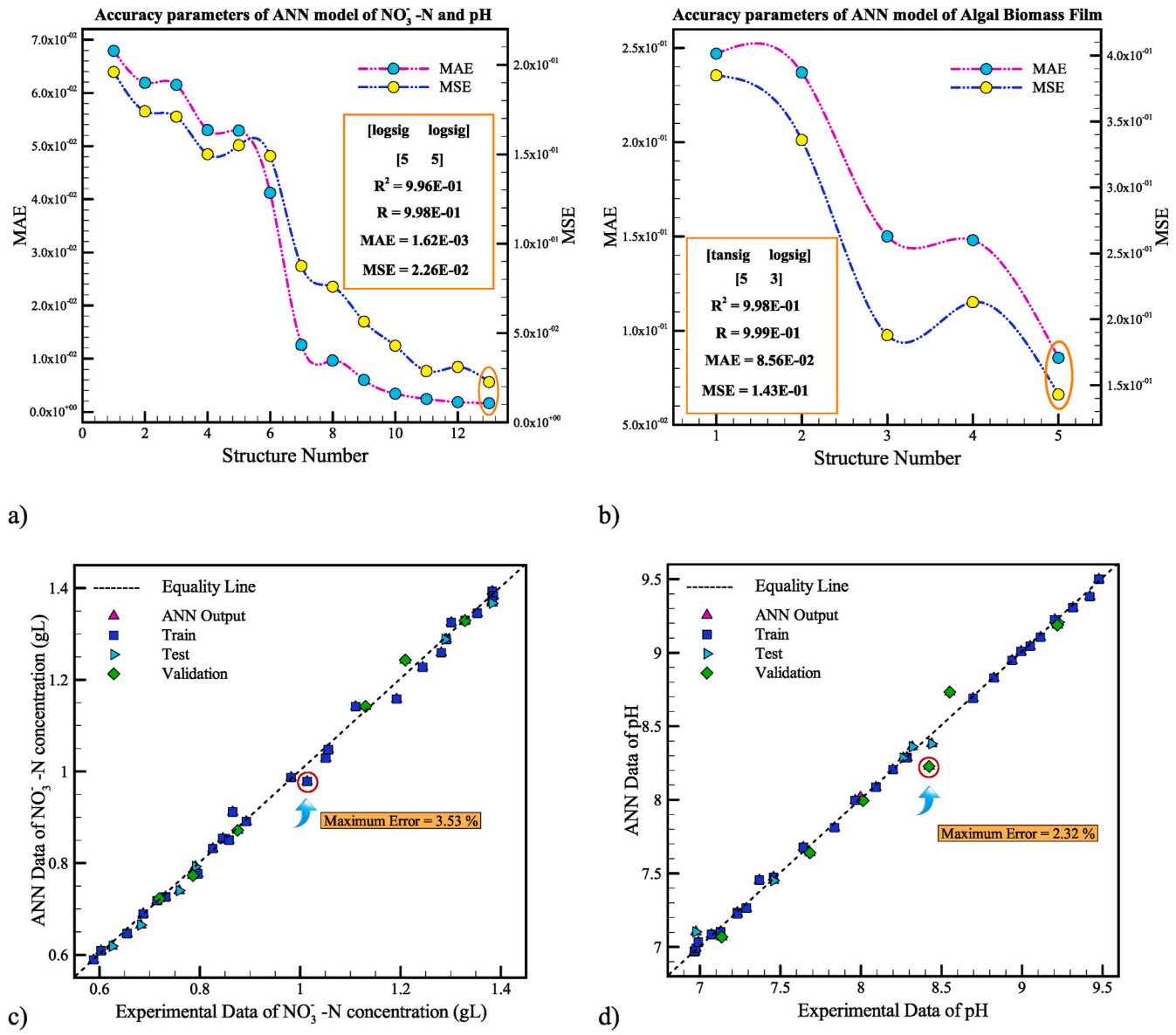

Fig. 6. Accuracy parameters of artificial neural network designed for a) NO_3–N concentration and pH. b) algal biomass film. Chart of matching of experimental data and predicted data by artificial neural network model for c) NO_3–N concentration (g/L), d) pH, e) algal biomass films (g/m^2). Residual graph of predicted data by artificial neural network model for f) NO_3–N concentration (g/L), g) pH, h) Algal biomass films (g/m^2).

02). Consequently, this model demonstrates accurate prediction capabilities for NO_3–N concentration and pH.

Fig. 6a and b displays a scatter plot featuring two distinct lines, one representing the MAE and the other representing the MSE. The x-axis is designated as "Structure Number," while the y-axis represents "MAE/MSE." The lines representing MAE and MSE are colored yellow and blue, respectively. The data points are visually represented as circular shapes. Based on the graphical representation, it can be shown that the ANN model, namely the one with a 5-5 structure, exhibits the highest level of accuracy. This is evident from the calculated metrics, including a mean absolute error of 1.62E-03, a MSE of 2.26E-02, and a R^2 of determination of 9.96E-01.

Furthermore, it is worth noting that the ANN model employed in this study for predicting Algal biomass film exhibits a 5-3 structure. Notably, this model demonstrates the highest level of accuracy, as seen by the following performance metrics: MAE of 8.56E-02, MSE of 1.43E-01, and a R^2 of 9.98E-01. Consequently, this model can effectively forecast NO_3–N concentration, pH levels, and Algal biomass film laboratory measurements.

Fig. 6c–e displays the most suitable distribution for three variables: a) concentration of NO_3–N (in grams per liter), b) pH level, and c) algal biomass films (in grams per square meter). The x-axis represents the experimental data, while the y-axis represents the data obtained from the ANN. Purple triangles, green squares, and blue diamond's represent data points. The black line, denoted as the "Equality Line," is the most suitable option. The red circle denoting "Max error" exhibits values of 12.18%, 3.53%, and 2.32% for the algal biomass films, NO_3–N concentration, and pH. The presented graphic demonstrates a strong agreement between the data generated by the neural network's predictions and the corresponding experimental data. The disparity between projected and experimental results is most pronounced in the case of algal biomass films but to a very negligible extent.

Consequently, the neural network model demonstrates a remarkable ability to forecast experimental results accurately. The results of AI modeling conform well with the other studies that used ANN for chemical process prediction and modeling because ANN modeling has

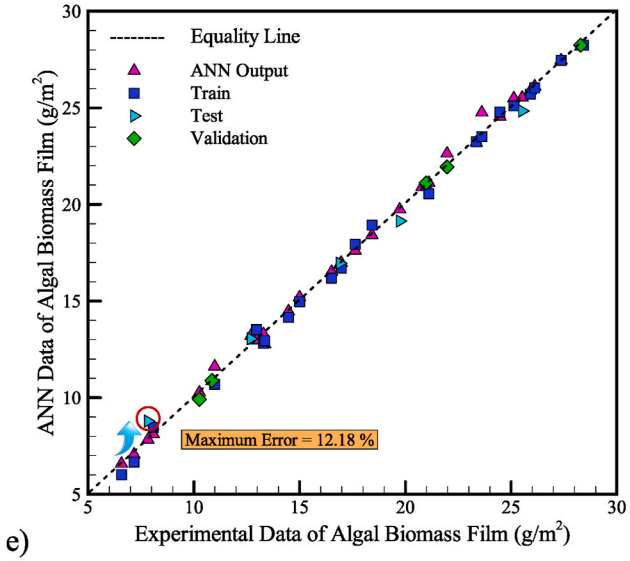

e)

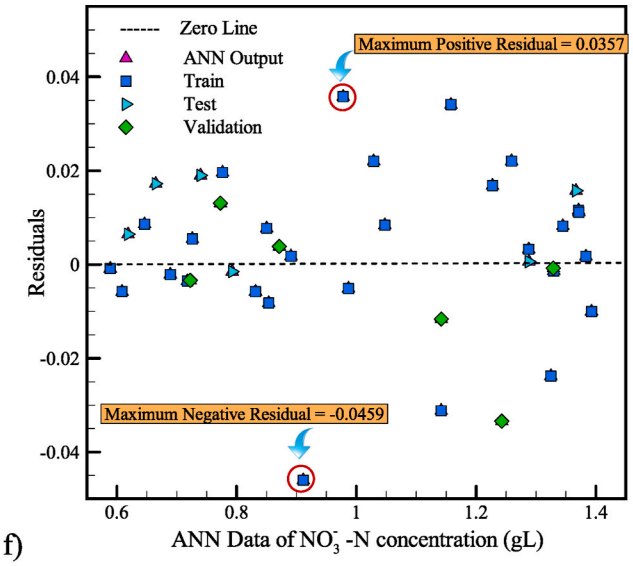

f)

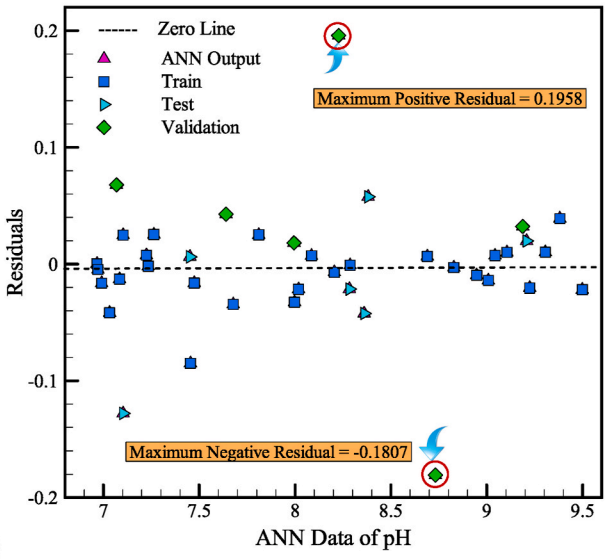

g)

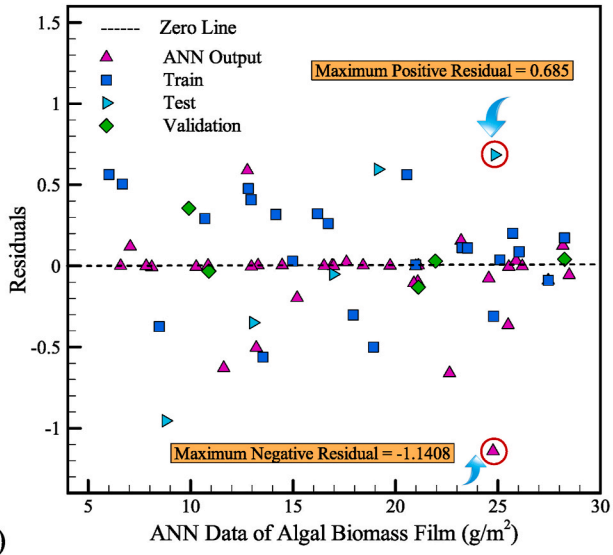

h)

Fig. 6. (*continued*).

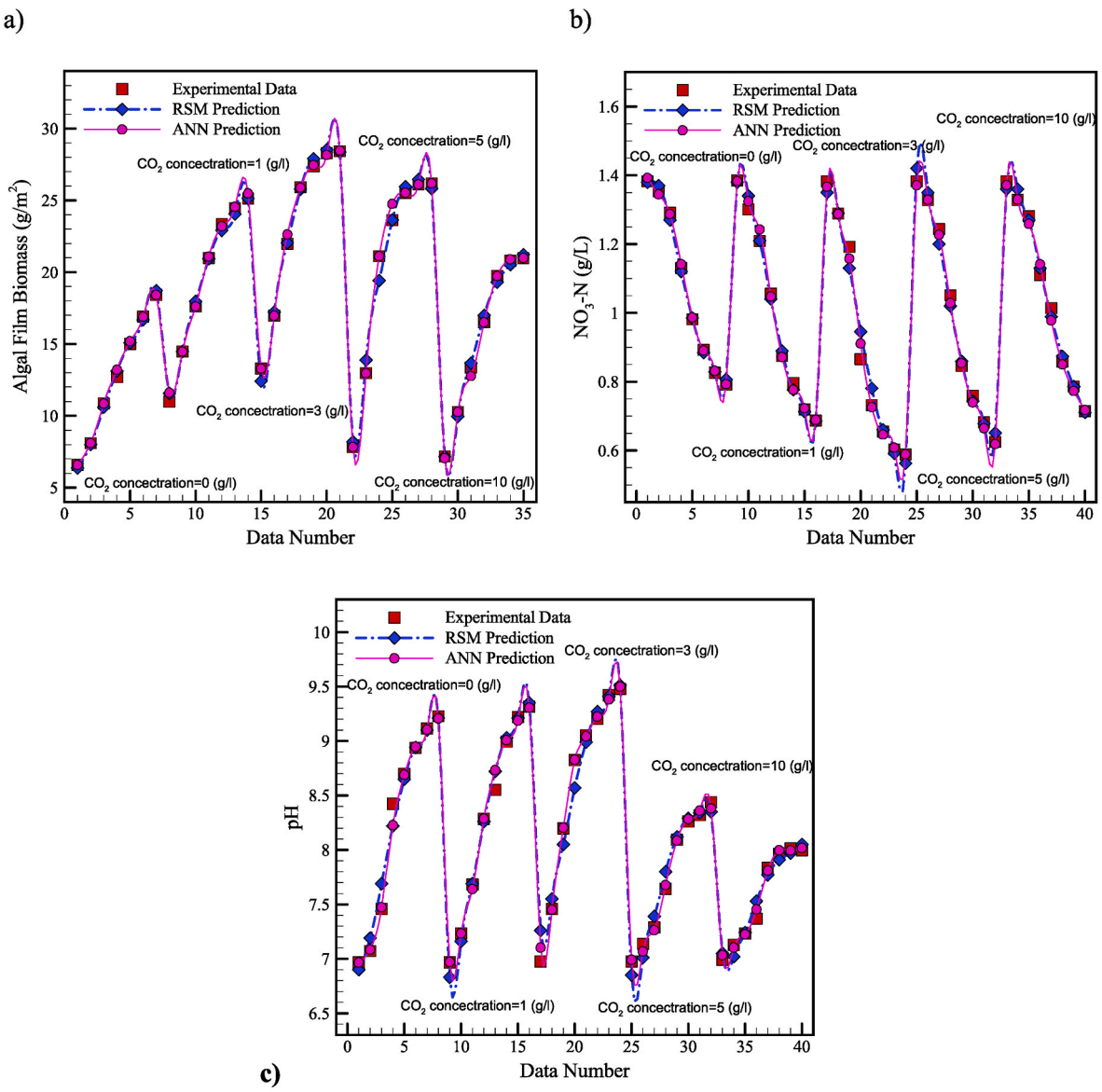

Fig. 7. Real-data comparison of RSM and ANN models for a) Algal Film Biomass and b) NO3–N c) pH.

shown good accuracy in predicting the process behavior according to experimental data.

The residual plan depicted in Fig. 6f-**h** exhibits a combination of green and blue data points accompanied by blue lines. The x-axis of the graph is labeled as "ANN data for a) concentration of NO_3–N (g/L), b) pH, and c) algal biomass film (g/m^2)", while the y-axis is designated as "Residual." At the y-coordinate of zero, a horizontal line is present on the plot, appropriately named the "Zero Line." The data represented by the purple triangles corresponds to the outputs of the ANN. The blue squares, on the other hand, depict the training data. The turquoise blue represents the test data, while the red circles symbolize the validation data. The residuals exhibit a dispersion pattern centered on the zero line, suggesting that the projected data lacks errors. The graph displays two labels indicating the maximum positive and negative residuals for three variables: a) NO_3–N concentration, b) pH, and c) Algal biomass film. The maximum positive residuals for these variables are 0.0357, 0.1958, and 0.685, respectively. Conversely, the maximum harmful residuals for these variables are −0.0459, −0.1807, and −1.1408, respectively. The graphical representation illustrates a strong concurrence between the estimated data generated by the neural network and the experimental data.

3.4. Comparing the outputs of RSM and ANN models

In this part, a comparison has been made between the data derived by the RSM and ANN models and the actual data collected from Algal Film Biomass, pH and NO_3–N. According to the results presented in Fig. 7-a, both models demonstrated high accuracy in predicting the experimental data for Algal Film Biomass. However, when the concentration of CO_2 increases, the neural network exhibited superior predictive capabilities compared to the RSM. This suggests that the neural network underwent more effective training. In Fig. 7-b, a comparison was made between the NO_3–N data, revealing that the ANN model had superior performance in this sector. The pH data of the proposed models are compared in Fig. 7-C. The presented figure demonstrates that, on the whole, the neural network model has exhibited superior predictive capabilities concerning the actual data, particularly in instances involving a concentration of 3 CO_2 and data points characterized by lower pH levels. Consequently, the ANN model exhibited enhanced performance for both data series.

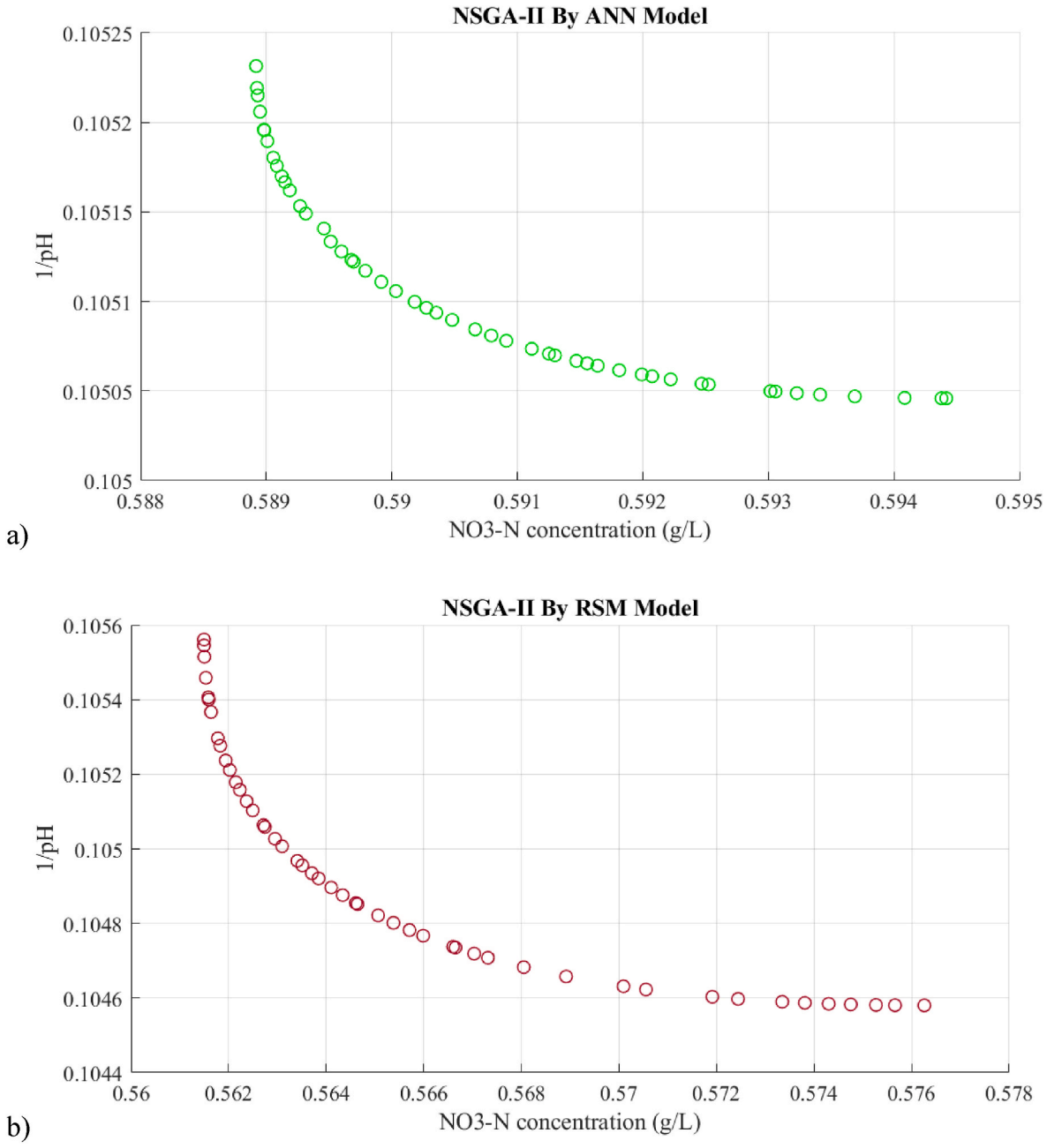

Fig. 8. Pareto front of optimization by a) ANN Model, b) RSM Model.

3.5. Optimization by NSGA-II

Fig. 8 a and **b** illustrates the utilization of the NSGA-II algorithm in conjunction with the ANN model and the RSM model to optimize laboratory data pertaining to NO_3–N concentration and pH. The x-axis is labeled as “concentration of nitrate ions (g/L)," while the y-axis is labeled as “inverse of pH.” The plotted data points exhibit a curvilinear pattern, originating from the upper left quadrant of the graph and gradually descending towards the lower right quadrant. This optimization aims to identify the optimal combination of NO_3–N concentration and pH that will deliver the maximum quality or quantity of a given product or process. Based on the graphical representation, it can be observed that the optimal position is situated at the point of intersection between the curve and its minimum value. The geographical area in question exhibits the most alkaline pH level and the least amount of NO_3–N concentration.

3.6. Comparison of this work with another

For this reason, efforts to meet the most accurate standards in quality and standardization will continue. One of the main problems is choosing the best algorithm for each process. Table 4 reviews recent work on modeling and optimizing the behavior of the algal membrane bioreactor process. Furthermore, Table 4 compares present work and other works in this field. As can be seen, the conformity of present study results with the results of recent studies is observed. However, the present study has examined different algorithms. One significant gap that must be noticed is trying different computational intelligence algorithms to find the best technique. In this regard, different algorithms have been examined in the present study.

Table 4
Overall review of recent work about modeling and optimization of algal membrane bioreactor process behavior.

Authors	Process	Technique	Results
Hajinajaf et al. (2022)	CO_2 Capture and Nutrient Removal by Microalgae Chlorella vulgaris	ANN & SVR	The Levenberg–Marquardt algorithm and Gaussian kernel with correlation coefficient values of 0.9937 and 0.9964 were selected as the optimal network.
Mojiri et al. (2022)	Contaminant Removal from Wastewater by Microalgal Photobioreactors	ANN	The high R^2 value (0.99) for both the removal of CAF and DEET denotes the reliability of the model.
Sharma et al. (2022)	Bio-hydrogen production using algal biomass	RSM	A validation testing shows that the biohydrogen production with a 4.52% error, which is fairly reasonable.
Sarkar et al. (2020)	Extraction of chlorophylls and carotenoids from dry and wet biomass of isolated Chlorella Thermophila	ANN	The modelling of the extraction process was performed using ANN which may be useful for the scale-up of the extraction process at the industrial level.
Present study	algal membrane bioreactor biomass and lipid production	RSM, ANN, NSGA-II	High accuracy in modeling with ANN and RSM. Also, successful optimization of process via using NSGA-II and RSM.

4. Conclusion and perspective

Both the RSM and the ANN were applied in this study to anticipate the algal biomass film, NO_3–N concentration, and pH. RSM stands for the RSM, and ANN is for the ANN. The models treated the CO_2 content and the passage of time as independent variables. The equations of the RSM model are applied to predict the temporal dynamics of algal biomass film, NO_3–N concentration, and pH while considering the influence of time and CO_2 concentration. An ANN is utilized as a modeling tool for algal biomass film. Its R^2 value is 9.98E-01, and its R-value is 9.99E-01.

Additionally, its MAE value is 8.56E-02, and its MSE value is 1.43E-01. The architecture of the network is described as having a 5-3 structure. As can be seen by its R^2 value of 9.96E-01, the R-value of 9.98E-01, MAE value of 1.62E-03, and MSE value of 2.62E-02, the ANN model has a high level of accuracy when it comes to forecasting NO_3–N concentration and pH. This is evidenced by the fact that these values are all minimal. The conditions were found to be most favorable for producing an algal biomass film at a CO_2 concentration of 2.884 mg/L and for some time equal to 6.589 days. At a CO_2 concentration of 2.984 mg/L and 6.787 days, the conditions were ideal for achieving the highest NO_3–N concentration and pH levels. These conditions led to the optimal conditions. The NSGA-II algorithm was used to optimize the identification of the ideal combination of NO_3–N concentration and pH to obtain the maximum possible yield or quality of a particular product or process. The goal of this endeavor was to optimize the identification of the optimal combination of NO_3–N concentration and pH. The NSGA-II algorithm suggests that the best position is the point on the curve where it reaches its minimum value. This point corresponds to the place on the curve with the highest pH level and the lowest concentration of NO_3–N. As the application of artificial intelligence in optimizing and modeling chemical processes becomes more recent, less effort and time spent on experimentation can be expected. However, it should not be forgotten that different algorithms have differences.

Funding

This research was funded by the Deanship of Scientific Research at King Khalid University under grant number RGP.2/34/44.

CRediT authorship contribution statement

Abdelfattah Amari: Funding acquisition, Writing - review & editing. **Noureddine Elboughdiri:** Writing - original draft, Writing - review & editing. **Esraa Ahmed Said:** Validation, Writing - original draft. **Sasan Zahmatkesh:** Conceptualization, Formal analysis, Investigation, Methodology, Software, Writing - original draft, Writing - review & editing. **Bing-Jie Ni:** Validation, Writing - original draft, Writing - review & editing.

Declaration of competing interest

The authors declare that they have no known competing financial interests or personal relationships that could have appeared to influence the work reported in this paper.

Data availability

The data that has been used is confidential.

Acknowledgments

The authors extend their appreciation to the Deanship of Scientific Research at King Khalid University for funding this work through Research Groups Program under grant number RGP.2/34/44.

Appendix A. Supplementary data

Supplementary data to this article can be found online at https://doi.org/10.1016/j.jenvman.2023.119761.

References

Agatonovic-Kustrin, S., Beresford, R., 2000. Basic concepts of artificial neural network (ANN) modeling and its application in pharmaceutical research. J. Pharmaceut. Biomed. Anal. 22 (5), 717–727.
Ahmad, F., 2022. Deep image retrieval using artificial neural network interpolation and indexing based on similarity measurement. CAAI Transactions on Intelligence Technology 7 (2), 200–218.
Aikhuele, D., 2023. Development of a statistical reliability-based model for the estimation and optimization of a spur gear system. Journal of Computational and Cognitive Engineering 2 (2), 168–174.
Amaro, H.M., Salgado, E.M., Nunes, O.C., Pires, J.C., Esteves, A.F., 2023. Microalgae systems-environmental agents for wastewater treatment and further potential biomass valorisation. J. Environ. Manag. 337, 117678.
Amiri, M.K., Zaferani, S.P.G., Emami, M.R.S., Zahmatkesh, S., Pourhanasa, R., Namaghi, S.S., Klemeš, J.J., Bokhari, A., Hajiaghaei-Keshteli, M., 2023. NSGA-II, ANN, MLP and ML. Multi-objective Optimization of Thermophysical Properties GO Powders-DW/EG Nf by RSM. Energy, 128176.
Asrami, M.R., Pirouzi, A., Nosrati, M., Hajipour, A., Zahmatkesh, S., 2023. Energy balance survey for the design and auto-thermal thermophilic aerobic digestion of algal-based membrane bioreactor under organic loading rates: experimental and simulation-based ANN and NSGA-II. Chemosphere, 140652.
Banerjee, S., Ghosh, D., Pandit, C., Saha, S., Mohapatra, A., Pandit, S., Sharma, M., Sridhar, K., Inbaraj, B.S., Prasad, R., 2023. Microalgal pandora for potent bioenergy production: a way forward? Fuel 333, 126253.
Bezerra, M.A., Santelli, R.E., Oliveira, E.P., Villar, L.S., Escaleira, L.A., 2008. Response surface methodology (RSM) as a tool for optimization in analytical chemistry. Talanta 76 (5), 965–977.
Bourquin, J., Schmidli, H., van Hoogevest, P., Leuenberger, H., 1998. Advantages of Artificial Neural Networks (ANNs) as alternative modelling technique for data sets showing non-linear relationships using data from a galenical study on a solid dosage form. Eur. J. Pharmaceut. Sci. 7 (1), 5–16.
Chen, H., Fu, Q., Liao, Q., Zhu, X., Shah, A., 2021. Applying artificial neural network to predict the viscosity of microalgae slurry in hydrothermal hydrolysis process. Energy and AI 4, 100053.
Garbowski, T., Pietryka, M., Pulikowski, K., Richter, D., 2020. The use of a natural substrate for immobilization of microalgae cultivated in wastewater. Sci. Rep. 10 (1), 7915.

Gasparin, A., Lukovic, S., Alippi, C., 2022. Deep learning for time series forecasting: the electric load case. CAAI Transactions on Intelligence Technology 7 (1), 1–25.
Gupta, P.L., Lee, S.-M., Choi, H.-J., 2015. A mini review: photobioreactors for large scale algal cultivation. World J. Microbiol. Biotechnol. 31, 1409–1417.
Hajinajaf, N., Fallahi, A., Rabbani, Y., Tavakoli, O., Sarrafzadeh, M.-H., 2022. Integrated CO2 capture and nutrient removal by microalgae Chlorella vulgaris and optimization using neural network and support vector regression. Waste and Biomass Valorization 13 (12), 4749–4770.
Hazrati, H., Moghaddam, A.H., Rostamizadeh, M., 2017. The influence of hydraulic retention time on cake layer specifications in the membrane bioreactor: experimental and artificial neural network modeling. J. Environ. Chem. Eng. 5 (3), 3005–3013.
Hu, X., Kuang, Q., Cai, Q., Xue, Y., Zhou, W., Li, Y., 2022. A coherent pattern mining algorithm based on all contiguous column bicluster. Journal of Artificial Intelligence and Technology 2 (3), 80–92.
Hussain, F., Shah, S.Z., Ahmad, H., Abubshait, S.A., Abubshait, H.A., Laref, A., Manikandan, A., Kusuma, H.S., Iqbal, M., 2021. Microalgae an ecofriendly and sustainable wastewater treatment option: biomass application in biofuel and bio-fertilizer production. A review. Renew. Sustain. Energy Rev. 137, 110603.
Ibrahim, S., Wahab, N.A., Ismail, F.S., Sam, Y.M., 2020. Optimization of artificial neural network topology for membrane bioreactor filtration using response surface methodology. IAES Int. J. Artif. Intell. 9 (1), 117.
Khan, J., Lee, E., Kim, K., 2022. A higher prediction accuracy–based alpha–beta filter algorithm using the feedforward artificial neural network. CAAI Transactions on Intelligence Technology.
Kleijnen, J.P., 2008. Response surface methodology for constrained simulation optimization: an overview. Simulat. Model. Pract. Theor. 16 (1), 50–64.
Meng, J., Li, Y., Liang, H., Ma, Y., 2022. Single-image dehazing based on two-stream convolutional neural network. Journal of Artificial Intelligence and Technology 2 (3), 100–110.
Mojiri, A., Ozaki, N., Kazeroon, R.A., Rezania, S., Baharlooeian, M., Vakili, M., Farraji, H., Ohashi, A., Kindaichi, T., Zhou, J.L., 2022. Contaminant removal from wastewater by microalgal photobioreactors and modeling by artificial neural network. Water 14 (24), 4046.
Myers, R.H., Montgomery, D.C., Vining, G.G., Borror, C.M., Kowalski, S.M., 2004. Response surface methodology: a retrospective and literature survey. J. Qual. Technol. 36 (1), 53–77.
Pendashteh, A.R., Fakhru'l-Razi, A., Chaibakhsh, N., Abdullah, L.C., Madaeni, S.S., Abidin, Z.Z., 2011. Modeling of membrane bioreactor treating hypersaline oily wastewater by artificial neural network. J. Hazard Mater. 192 (2), 568–575.
Sarkar, S., Manna, M.S., Bhowmick, T.K., Gayen, K., 2020. Extraction of chlorophylls and carotenoids from dry and wet biomass of isolated Chlorella Thermophila: optimization of process parameters and modelling by artificial neural network. Process Biochem. 96, 58–72.
Schmitt, F., Banu, R., Yeom, I.-T., Do, K.-U., 2018. Development of artificial neural networks to predict membrane fouling in an anoxic-aerobic membrane bioreactor treating domestic wastewater. Biochem. Eng. J. 133, 47–58.
Schmitt, F., Do, K.-U., 2017. Prediction of membrane fouling using artificial neural networks for wastewater treated by membrane bioreactor technologies: bottlenecks and possibilities. Environ. Sci. Pollut. Control Ser. 24 (29), 22885–22913.
Schultze, L.K., Simon, M.-V., Li, T., Langenbach, D., Podola, B., Melkonian, M., 2015. High light and carbon dioxide optimize surface productivity in a Twin-Layer biofilm photobioreactor. Algal Res. 8, 37–44.
Sharma, P., Sivaramakrishnaiah, M., Deepanraj, B., Saravanan, R., Reddy, M.V., 2022. A novel optimization approach for biohydrogen production using algal biomass. Int. J. Hydrogen Energy.
Su, Z., Sharma, M., Zhang, P., Zhang, L., Xing, X., Yue, J., Song, Z., Nan, L., Yujun, S., Zheng, Y., 2023. Bimolecular transitions and lipid synthesis in marine microalgae for environmental and human health application. J. Environ. Chem. Eng., 110398
Wang, X., Wang, S., Chen, P.-Y., Lin, X., Chin, P., 2020. Block Switching: a Stochastic Approach for Deep Learning Security arXiv preprint arXiv:2002.07920.
Yang, C., Cavalcante, J., de Freitas, B.B., Lauersen, K.J., Szekely, G., 2023. Crude algal biomass for the generation of thin-film composite solvent-resistant nanofiltration membranes. Chem. Eng. J. 470, 144153.
Yen, H.-W., Hu, I.-C., Chen, C.-Y., Nagarajan, D., Chang, J.-S., 2019. Design of photobioreactors for algal cultivation. Biofuels from Algae. Elsevier, pp. 225–256.
Zahmatkesh, S., Gholian-Jouybari, F., Klemeš, J.J., Bokhari, A., Hajiaghaei-Keshteli, M., 2023. Sustainable and optimized values for municipal wastewater: the removal of biological oxygen demand and chemical oxygen demand by various levels of geranular activated carbon-and genetic algorithm-based simulation. J. Clean. Prod. 417, 137932.
Zhang, L., Wang, Y.-Z., Wang, S., Ding, K., 2018. Effect of carbon dioxide on biomass and lipid production of Chlorella pyrenoidosa in a membrane bioreactor with gas-liquid separation. Algal Res. 31, 70–76.
Zhang, Z., De Luca, G., Archambault, B., Chavez, J., Rice, B., 2022. Traffic dataset and dynamic routing algorithm in traffic simulation. Journal of Artificial Intelligence and Technology 2 (3), 111–122.